
Finding Pegasus: Enhancing Unsupervised Anomaly Detection in High-Dimensional Data using a Manifold-Based Approach

R.P. Nathan¹ Nikolaos Nikolaou¹ Ofer Lahav¹

Abstract

Unsupervised machine learning methods are well suited to searching for anomalies at scale but can struggle with the high-dimensional representation of many modern datasets, hence dimensionality reduction (DR) is often performed first. In this paper we analyse unsupervised anomaly detection (AD) from the perspective of the manifold created in DR. We present an idealised illustration, ‘Finding Pegasus’, and a novel formal framework with which we categorise AD methods and their results into ‘on manifold’ and ‘off manifold’. We define these terms and show how they differ. We then use this insight to develop an approach of combining AD methods which significantly boosts AD recall without sacrificing precision in situations employing high DR. When tested on MNIST data, our approach of combining AD methods improves recall by as much as 16% compared with simply combining with the best standalone AD method (Isolation Forest), a result which shows great promise for its application to real-world data.

1. Introduction

When it comes to availability of data, this is a golden age for researchers across a multitude of disciplines, offering huge potential to make new discoveries (find ‘unknown unknowns’), confirm existing or evolving theory, and highlight problems with data collection and processing. The search for unusual or anomalous data instances is therefore a key research focus, but the sheer volume of data available combined with the high-dimensional (high-D) format in which they are often captured, mean it can be a challenge to find anomalous instances hidden within them. These challenges have led to machine learning techniques being employed to look for anomalies at scale. In partic-

¹Centre for Doctoral Training in Data Intensive Science, University College London, Gower St, London WC1E 6BT, UK. Correspondence to: R.P. Nathan <ucaprn@ucl.ac.uk>.

ular, unsupervised approaches are well suited to the task of finding outliers in a population of data without need for pre-labelling. Their flexibility, relative ease of implementation and the wide range of available models means unsupervised anomaly detection (AD) is employed across many fields of research. As we shall see, however, unsupervised approaches tend to struggle with high-D data, and as a result dimensionality reduction (DR) is often performed directly or indirectly to produce a simpler representation of the data prior to analysis for anomalies. In doing this, a lower-dimensional manifold is created. In this paper we seek to reframe the AD problem in high-D data and encourage the reader to regard it from the perspective of this manifold.

Our paper is organised as follows. In Section 2 we provide a summary of AD concepts and terminology, and describe how the ‘Curse of Dimensionality’ makes this task more onerous in high-D representations. In Section 3 we see how DR is used to mitigate these issues and how the manifold thereby created is central to AD. In Section 4 we provide an idealisation of AD using DR – ‘**Finding Pegasus**’ – to illustrate one of this paper’s main concepts, that of AD methods working either ‘**on manifold**’ or ‘**off manifold**’. Section 5 approaches the topic more rigorously and provides a novel formal framework for AD with high-D data and shows how this understanding enables us to boost recall. **To the best of our knowledge, this is the first time the AD problem has been formulated in this way.** Finally, in Section 6 we summarise the results of applying these concepts to MNIST handwritten digits. Where it is occasionally helpful to illustrate the concepts being discussed with a real-world example of high-D data, we shall use the example of astronomical spectra collected as part of a large galaxy survey.

2. Anomaly Detection (AD) in High-D

2.1. AD Prerequisites

Ruff et al. (2020) define an anomaly as ‘an observation that deviates considerably from some concept of normality’, and we shall adopt that definition in this paper. In AD literature, there is often also a distinction drawn between ‘outliers’ and ‘novelties’. The former is used for ob-

servations which are considered extreme or isolated within a training set of data. By contrast, the latter term is reserved for a new observation, for which similar instances were not present within the training set. In this context, outlier detection is considered an unsupervised activity, i.e. one in which the data does not need to be pre-labelled; whereas novelty detection might be considered supervised or semi-supervised. This work focuses on unsupervised outlier detection, though many of the conclusions may be more broadly applicable, and throughout this paper we shall use the terms ‘outlier’ and ‘anomaly’ interchangeably.

Ruff et al. (2020) also provide a probabilistic definition of anomalies following similar treatments by Edgeworth (1887), Barnett and Lewis (1994) and others. Letting $X \subseteq \mathbb{R}^D$ be the data space of dimensionality D associated with some application, they define the ‘concept of normality’ for this application as the distribution \mathbb{P}^+ on X . This represents the ‘ground-truth’ law of normal behaviour in this application. Correspondingly, an anomaly will be an observation $x \in X$ that is in a low probability region of \mathbb{P}^+ and hence deviates significantly from the law of normality. They then define a set of anomalies, A , as:

$$A = \{x \in X | p^+(x) \leq \tau\}, \quad \tau \geq 0 \quad (1)$$

where p^+ is the probability density function corresponding to \mathbb{P}^+ , and τ is a threshold set so that the probability of A under \mathbb{P}^+ is below a requisite level.

Where we have a ‘ground-truth’ knowledge of the data, it is possible to score the efficacy of one AD method over another in terms of standard metrics of recall, precision and F1 score as defined in Appendix A.

2.2. The Curse of Dimensionality

Whilst a probabilistic approach might be helpful in certain circumstances, it can be rendered impracticable where the data is represented in high-D. This is the case for many domains of research. In our astronomy example, galaxy surveys typically collect the spectra of target objects across thousands of small wavelength bins, e.g. those collected by the Dark Energy Spectroscopic Instrument (DESI Collaboration et al., 2016) are captured across ≈ 7800 bins, hence they are effectively 7800D. High-D data like this means we are more likely to be afflicted by the Curse of Dimensionality (Bellman, 1966) which impacts data distributions and densities. More background is given in Appendix B but for our purposes it is sufficient to note that data points become more sparse in high dimension and so the concept of nearest neighbours starts to fail. Distributions (e.g. Gaussians), also behave differently in high dimension to our experience from low (one or two) dimensional representations. These factors have an impact on unsupervised AD methods which often rely on estimates of

nearest neighbours or measurements of local concentration to determine outliers.

This is illustrated by Han et al (2022) in a comprehensive benchmarking of AD methods available through `PyOD` (Zhao et al., 2019, a Python library for detecting anomalous/outlying objects in multivariate data) and `scikit-learn` (Pedregosa et al., 2011). Review of their detailed results (in particular Table D4 from Han et al. 2022) showed that, in general, none of the unsupervised AD methods tested performed particularly well with the higher-D datasets in the benchmarking sample. A solution to this would seem to be to transform the dataset into a lower-dimensional (low-D) representation before searching for anomalies. This might occur implicitly, e.g. by downsampling or feature selection, or explicitly using the approaches described in Section 3.1.

3. Dimensionality Reduction (DR)

Meaningful data compression through DR relies on the ‘Manifold Hypothesis’ (e.g. Goodfellow et al. 2016) that most real-world high-D datasets actually reside close to a (much) lower-D manifold which can well represent the bulk of the points in the dataset. An M -dimensional manifold is part of D -dimensional space ($M < D$) that locally resembles an M -dimensional hyperplane, i.e. the surface resembles Euclidean space locally. Points can be considered **well represented by the manifold** if there is only a small error, below some threshold, arising when we attempt to reconstruct the original high-D representation of the point from the manifold representation using whatever metric was implicit in the manifold’s creation. Similarly, we can define a **good manifold** as one which well represents the bulk of the points considered normal in the dataset. By definition, a good manifold will satisfy the manifold hypothesis.

For example, in the case of extracting useful information from astronomical spectra, there is a body of research which shows one can construct a lower-dimensional manifold from the original high-D representation which well captures the physical properties of spectra i.e. that the manifold hypothesis is valid. Yip et al. (2004a) found the first 3 PCA (see below) components could be used to separate different types of galaxies. Yip et al. (2004b) also found, however, that non-linear features, e.g. from quasars, required ~ 50 PCA components to effectively represent them. For features such as these, non-linear methods might be preferred and could be very effective, e.g. Portillo et al. (2020) used a variational autoencoder (VAE, see below) to reconstruct spectra well from the Sloan Digital Sky Survey (SDSS) with a manifold of only 6 latent parameters.

3.1. Determining the Manifold

The two main approaches to determine an appropriate lower-dimensional manifold are projection and manifold learning.

Projection is a linear approach which assumes the data resides on or close to a lower-dimensional hyperplane in the original high-D space. The most common projection method is Principal Component Analysis (PCA, e.g. Bishop 2007), a statistical technique which linearly transforms the data into a new coordinate system defined by orthogonal axes which are chosen to explain as much of the variation in the data as possible. Randomized search may be used to obtain the optimal number of dimensions.

Manifold Learning does not presume the shape of the manifold but instead attempts to learn it through parametric or non-parametric means. This approach will be advantageous where the manifold shape is more complex than a simple hyperplane. Examples of manifold learning methods include Local Linear Embedding (Roweis & Saul, 2000), t-SNE (van der Maaten & Hinton, 2008), Autoencoder (AE) (Kramer, 1991) and Variational Autoencoder (VAE) (Kingma & Welling, 2022). More detail on these techniques is given in Appendix D.1

3.2. Model Dependence of the Manifold

The exact manifold we construct will depend on the approach used, e.g. PCA will produce an M -dimensional hyperplane whereas AEs or VAEs produce more complex M -dimensional surfaces in D -dimensional space. Since the manifold is model-dependent, it follows that the **anomalies detected using it must also be model-dependent**.

3.3. Using the Manifold for AD

There are essentially two ways by which AD techniques use the low-D manifold to identify outliers within a population. (See Appendix C for a schematic summary of this.)

The first approach is to look for points which are isolated or extreme in the low-D manifold representation of the distribution, typically because of distance from neighbouring points, or relative under-density of surrounding points. It will be helpful to refer to methods working in this way as **on-manifold methods** and the anomalies which are detected using them as **on-manifold anomalies**. Examples of such methods include Gaussian Mixture Model (e.g. Géron 2023), K-Nearest Neighbours (Ramaswamy et al. 2000), Local Outlier Factor (LOF, Breunig et al. 2000), Elliptic Envelope (EE, Rousseeuw & Driessen 1999), One-Class Support Vector Machine (OCSVM, Schölkopf et al. 1999), and Isolation Forest (IF, Liu et al. 2008). Details of these techniques are given in Appendix D.2.

The second approach leverages the low-D manifold in a different way. Since the bulk of the dataset is well represented by the manifold, poorly represented points can be assumed to be outliers. We find these by looking for points with a high error between the original high-D representation and its reconstruction from the manifold representation employing whatever metric was used in the manifold’s creation. We shall refer to these methods as **off-manifold methods** and the anomalies which are detected using them as **off-manifold anomalies**. Examples of such methods include reconstruction error from PCA, AE and VAE manifolds.

3.4. On Manifold vs Off Manifold

During compression to the lower-dimensional representation, some anomalous points might end up in the body of the low-D distribution rather than in extreme or isolated positions, hence on-manifold methods may not find them. This will be a particular concern when the features which make the observations abnormal are not well correlated to the features which remain after DR has been applied. Another way to think of that is that information essential to distinguishing an anomaly from a normal point is lost when the data representation undergoes compression.

Conversely, in the reconstruction approach, anomalous points which are somehow well-represented by the manifold but are in extreme or isolated positions on it, will not show significant reconstruction error and therefore will not be detected by an off-manifold method.

If manifold construction is physically informed, then we might be able to more easily ascribe physical meaning to the extreme points on it, and we might find these with an on-manifold method. **Hence, we might expect on-manifold anomalies to be extremes in our current thinking. Conversely, off-manifold anomalies might be where we would hope to find new science, i.e. unknown unknowns.**

Regarding the problem from the perspective of the manifold, we see there can be a difference between on- and off-manifold anomalies. If the objective is to detect as many anomalies as possible – as it often is in discovery-driven fields – then a useful approach would seem to be to **combine complementary on- and off-manifold methods thereby maximising the superset of anomalies which are detected**. By ‘complementary’ we mean that we would employ the same manifold for both the on- and off-manifold methods.

Many researchers, mindful of the No Free Lunch Theorem (Wolpert, 1996), use an ensemble of unsupervised AD techniques, thereby creating a superset of anomalies for subsequent analysis. By considering the problem from the perspective of the manifold created by DR, however, we

should be able to make more informed and efficient choices about the AD methods we use.

4. Finding Pegasus

We now present a simplified illustration of AD using DR. Consider an idealized horse dataset with two features, these being horse height and weight. From everyday experience we would anticipate good correlation between horse height and weight, so when plotted we might expect these data to form a distribution like the grey shaded area in Fig. 1.

Consider within this dataset a pair of interesting outlying points. To the left of Fig. 1 is an artist’s impression of *Eohippus*, a precursor to the modern horse, thought to have been 20-30cm high. On the right is a depiction of *Sampson*, thought to have been the biggest ever horse, measured at 2.2m to the shoulder. Both horses, though extreme in size, still fit in well with the overall expectation that height and weight are highly correlated.

We now add a third feature to the dataset, this being the number of pairs of wings the horse possesses (taking values either 0 or 1). Naturally, the existing points in the horse dataset will be unaffected by the inclusion of this extra attribute, so we add one more point to the dataset which will act as an outlier with respect to this feature. And this point, *Pegasus*, the winged horse of Greek mythology, is also shown in Fig. 1.

4.1. DR from 3D to 2D

Our task is to find anomalies in our dataset. Let us assume we need to first reduce the dimensionality of the dataset down to 2D. We choose PCA for this task. The resulting lower-dimensional manifold which is created using PCA will be a hyperplane almost coincident with the height-weight plane.

When we compress the dataset onto this plane, most of the points, *Eohippus* and *Sampson* included, will be largely unchanged, since they essentially already sit on the lower-dimensional manifold (\approx height-weight plane). The point representing *Pegasus*, however, will be projected into the heart of the data distribution given its average height and weight and assuming its (magical) wings are weightless.¹

¹Declaring *Pegasus*’s wings to be weightless implies that this new attribute is not well correlated with existing features of the dataset, i.e. height and weight. If *Pegasus*’s wings had instead been very heavy, then its total weight would have pushed its projection out of the bulk of the distribution and placed it in a lower-density region.

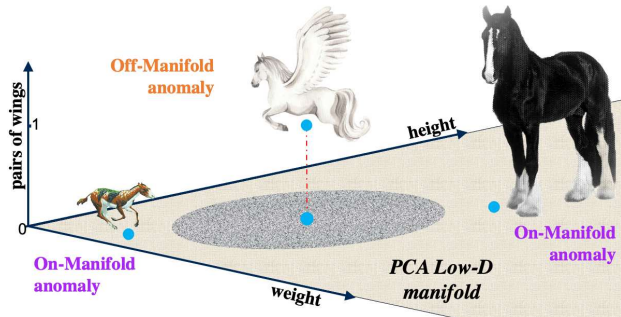


Figure 1. AD using idealised Finding Pegasus dataset illustrating the distinction between on- and off-manifold anomalies. (Horse images created using Canva.com)

4.2. Performing AD with the Manifold

We first perform **on-manifold** AD. We use Local Outlier Factor to find points which are in areas of relatively low density. We should find *Eohippus* and *Sampson* with relative ease, since they sit apart from the bulk of the data. We are unlikely to find *Pegasus*, however, because as noted above, its projection onto the manifold has placed it in the heart of a concentration of other points representing horses of average weight and height.

Next we perform **off-manifold** AD, and we will look for points which are poorly represented by the low-D manifold. When we try to reconstruct the original representation of these points from their low-D manifold representation there will be a large error. In the case of PCA, the metric used to construct the manifold is mean squared error (MSE). So, in this case, outliers will simply be those points for which the original representation is far from the 2D manifold representation. Using this approach, we should easily find *Pegasus* as an outlier. But we are unlikely to detect *Eohippus* and *Sampson* as outliers because their projection onto the manifold is almost coincident with their original representation, and so will have near-zero reconstruction error.

The *Eohippus* and *Sampson* outliers found on manifold represent extremes in our current view of what a horse can be; whereas *Pegasus*, found off manifold, is a different kind of horse entirely – new science. All these anomalies would likely be of interest to us, and by combining complementary (i.e. using the same manifold) on- and off-manifold methods should allow us to detect all three. Henceforth, we shall refer to this as the ‘**Finding Pegasus Approach**’.

Had there been high correlation between wing weight and body weight (i.e. if *Pegasus* had had heavy wings rather than magical, weightless, wings) then we might have been able to detect *Pegasus* on manifold. But because of high reconstruction error we would also have been able to detect the anomaly off manifold. Hence, in general, we do

not expect the sets of anomalies found on manifold and off manifold to be disjoint.

5. Formal Framework for AD in High-D Data

5.1. Raw Data Representation

We now introduce a simple, and we believe novel, formal framework that we have devised to describe AD in high-D data. An overview of this framework is shown in Fig. 2, and illustrative applications are provided in Appendix F.

As per Section 2 we let $X \subseteq \mathbb{R}^D$ be the data space of high dimensionality D associated with some application. The sample X consists of N **normal** points and A **detectable anomalous** points, where N and A are disjoint, i.e. $X = N \cup A$ and $N \cap A = \emptyset$.

We regard the anomalies, A , as the set of points which deviate considerably from the concept of normality for our application; and conversely N are the points which are in accordance with it. By saying the points in A are detectable, we mean that there is enough information contained in the raw D -dimensional representation of the dataset that a domain expert with requisite tools and time would be able to identify the points as being abnormal. Additionally, from the general definition provided by (Ruff et al., 2020), we can assume $|N| \gg |A|$.

5.2. DR

We now reduce the dimensionality of the data representation of X from D to M dimensions, where $M < D$. In practice we would effect this by using methods of the type described in Section 3. We shall call this low-D representation X' .

In X' , some points will be well-represented by the manifold and some will not. We shall denote points which are well represented with a subscript of ‘+’; and points which are poorly represented by ‘-’. As per Section 3, points will be considered well-represented by the manifold if there is only a small error arising when we attempt to reconstruct the original representation of the point from the manifold representation using whatever metric was implicit to the manifold’s creation. Hence, we can write

$$X' = (N_+ \cup N_-) \cup (A_+ \cup A_-), \quad (2)$$

where $N_+ \cap N_- = A_+ \cap A_- = \emptyset$ and for avoidance of doubt $|X'| = |X|$. Rearranging Equation 2 we get

$$X' = (N_+ \cup A_+) \cup (N_- \cup A_-), \quad (3)$$

where the first bracket on the right hand side contains the disjoint sets of points in X' which are well-represented by

the manifold, and the second bracket contains the disjoint sets of points which are poorly represented.

5.3. Anomalies in Reduced Dimensionality

5.3.1. DETECTABLE AND UNDETECTABLE INSTANCES

Equation 3 indicates how *well* the sets of normal and anomalous points, as labeled in the original D -dimensional data space, are represented by the M -dimensional manifold. It does not say how *detectable* the anomalous points will be in lower dimension. The reduction in dimensionality is a compression of the data space, and information must be lost as a result of this compression unless there was significant redundancy in the original representation. Hence we would expect that fewer of the anomalies will be detectable in lower dimension. If A is the original set of detectable anomalies, we can write

$$A' = A_d \cup A_u, \quad A_d \cap A_u = \emptyset, \quad (4)$$

where A' is the representation on the M -dimensional manifold of the anomalous points which were detectable in D dimensions, and for the avoidance of doubt $|A'| = |A|$. A_d are those points which are still detectable as anomalies in the lower-dimensional representation; and A_u are those points for which there is now insufficient information to distinguish them from points considered normal. A_d and A_u are disjoint by definition.

The reduction in dimensionality will also sufficiently impact some normal points to make them now appear anomalous. If N was the original subset of normal points, and N' their representation in M dimensions, we can write

$$N' = N_N \cup N_d, \quad N_N \cap N_d = \emptyset, \quad (5)$$

where for avoidance of doubt $|N'| = |N|$. N_N are points which are still identifiable as normal points in the low-D representation, and N_d are points which now appear to be anomalies and would be regarded as false positives if detected through an AD process.²

5.3.2. IMPLICATIONS OF A GOOD MANIFOLD

We assume that efforts have been made to construct a good manifold (see Appendix E for how this might be relaxed), hence the manifold hypothesis holds for our application. From Section 3, we can assume $|N_+| \gg |N_-|$, i.e. that most of the points we consider to be normal will be well-represented by the manifold; and that $|N_N| \gg |N_d|$, i.e. that few normal points will appear anomalous in the low-D

²A more extensive discussion of detectability in reduced dimensionality is provided in Appendix E.

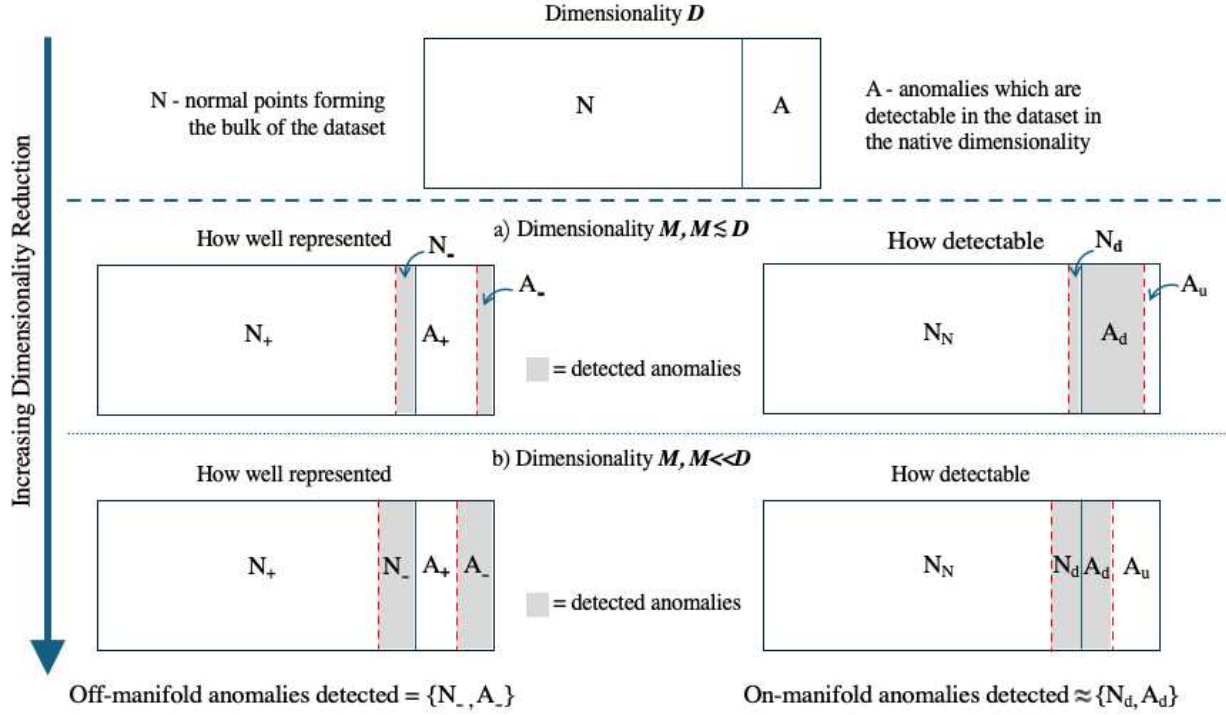


Figure 2. Schematic of formal framework for AD using DR. Detected off- and on-manifold anomalies are shown by the shaded regions.

representation, regardless of the scale of DR applied (see Section 5.4). It does not follow that we can assume the same relationships hold for anomalous points since our definition of a good manifold is centred on how well it represents normal points. We know, however, from Equation 2 that $A' = A_+ \cup A_-$ and so combining with Equation 4 we are then able to say

$$A_+ \cup A_- = A_d \cup A_u, \quad (6)$$

i.e. that the union of the (disjoint) sets of well and poorly represented anomalous points will equal the union of the (disjoint) sets of anomalous points detectable on the low-D manifold and those no longer detectable. For avoidance of doubt, we note that in general $A_+ \neq A_d$ and $A_- \neq A_u$.

5.4. How Much DR?

We noted in Section 5.3.2 that we will be applying a level of DR such that the manifold hypothesis holds. Hence, we have implicitly assumed values for M which allow for faithful reconstruction of the bulk of the population. But we have thus far placed no explicit constraint on the size of M other than $M < D$. Going forward, it will be instructive to consider two regimes for M , the first where $M \lesssim D$ i.e. scenarios where M is smaller than D but of the same order of magnitude; and the second where $M \ll D$.

If $M \lesssim D$ then we would straightforwardly expect $|A_-| \ll |A_+|$. The reduction in dimensionality of the dataset has been modest, hence we would expect only a minimal number of anomalous points to change from being well-represented in the native dimensionality (which all points are by definition) to being poorly represented. Another way of saying this is that if the level of DR is small, then $|N_+| \gg |N_-|$ holds not just because of the manifold hypothesis, but because little has changed in terms of representation. And that should be the case for anomalous points as much as for normal points. Following a similar argument, we would also expect $|A_u| \ll |A_d|$. And, in the limit that $M \rightarrow D$, we would expect $|A_-| \rightarrow 0$ and $|A_u| \rightarrow 0$.

If $M \ll D$ then significant DR has now been performed. We assume the manifold hypothesis still holds, hence $|N_+| \gg |N_-|$. As noted in Section 5.3.2, it does not follow that we can write the equivalent relationship for anomalous points. It would be reasonable, however, to assume that the number of anomalies which are poorly represented by this manifold is now significant, and to write the loose constraint that $|A_-| \approx |A_+|$. And, following a similar argument, we would also expect $|A_u| \approx |A_d|$.

5.5. AD in Reduced Dimensionality

5.5.1. ON-MANIFOLD ANOMALIES

We now look for anomalies in the compressed dataset. First, we employ a model to detect anomalies on the M -dimensional manifold. This will detect A_{mod}^* candidate anomalies, which will be a mixture of anomalies (true positives) and normal points (false positives). Hence our set of candidate on-manifold anomalies will be

$$A_{on}^* = A_{mod}^* = A_{mod} \cup N_{mod}, \quad (7)$$

where A_{mod} are the true positives and N_{mod} the false positives found by the model. We can define a **good model** to be one for which $A_{on}^* \approx A_d \cup N_d$. i.e. a good model can detect most of the anomalies which are still detectable in the compressed representation on this manifold. This is not a violation of the no free lunch theorem since we require this particular model to be effective for this particular manifold representation of this particular dataset and not in general.

Since the manifold hypothesis is assumed to hold, i.e. $|N_N| \gg |N_d|$ regardless of whether $M \lesssim D$ or $M \ll D$, but is assumed not to apply to anomalous points, it is reasonable to assert that $|N_d| \gg |A_d|$. As such, expert review of the set of on-manifold candidate anomalies, restored to their original dimensionality if necessary, should be feasible to identify the true anomalies. Hence, for a good model:

$$A_{on} = A_{mod} \approx A_d. \quad (8)$$

We note, however, that from Section 2.2 that we are less likely to easily meet this definition if $M \lesssim D$ since unsupervised methods can struggle with high-D data.

Since the model is detecting anomalies based on their manifold representation, it is reasonable to assume that the anomalies which a good model would be best at finding should be similar to the set of those anomalous points which are well represented by the manifold. Hence,

$$A_{on} = A_{mod} \approx A_d \approx A_+, \quad (9)$$

i.e. using a good on-manifold model will allow us to detect on-manifold anomalies approximately equal to the set of anomalies which remain detectable in the lower-dimensional representation, and these should be similar to the set of well-represented anomalies.

5.5.2. OFF-MANIFOLD ANOMALIES

Anomalies which are poorly represented by the M -dimensional manifold – the off-manifold anomalies – will

be detectable by looking for points with high reconstruction error based on whatever metric was implicit in manifold construction. This should yield a set of candidate anomalies, A_{off}^* , which are a mixture of both normal and anomalous points, the contents of the second bracket in Equation 3, i.e.

$$A_{off}^* = N_- \cup A_-. \quad (10)$$

We know $|N| \gg |A|$ and $|N_+| \gg |N_-|$ hence both $|N_-|$ and $|A_-|$ are small compared with the overall size of X' . Hence, expert review of the set of off-manifold candidate anomalies, restored to their original dimensionality if necessary, should be feasible to distinguish normal points from anomalous ones, thereby giving us the number of off-manifold anomalies $A_{off} = A_-$, i.e. off-manifold anomalies are simply the set of anomalous points which are poorly represented by the manifold.

5.5.3. THE FINDING PEGASUS APPROACH

Let us now combine on- and off-manifold anomalies using the two regimes of the scale of DR as described in 5.4.

a) $M \lesssim D$: We know that as $M \rightarrow D$, $A_{off} = A_- \rightarrow \emptyset$ and $A_+ \rightarrow A'$. Thus from Equation 9 we see that when there is only small DR, $A_{on} \approx A'$ for a good model and the contribution from A_{off} will be small. Hence, combining off-manifold anomalies with on-manifold anomalies would not be expected to increase recall significantly. And Section 2.2 remind us that unsupervised methods struggle in high-D, so we do not expect recall from A_{on} to be high in general when raw dimensionality is high.

b) $M \ll D$: From Equation 8 and since $A_{off} = A_-$ we see that for a good model, the Finding Pegasus Approach would detect anomalies

$$A_{det} = A_{on} \cup A_{off} \approx A_d \cup A_-. \quad (11)$$

We know that $|A_-| \approx |A_+|$ when significant DR has been applied and that $|A_{off}| = |A_-|$. We have also already seen that $A_{on} \approx A_+$. Hence $|A_{on}| \approx |A_{off}|$ when there has been significant DR. Therefore, **relying solely on on-manifold methods will create an effective ceiling on recall where significant DR has been applied.** In addition, **combining complementary off- and on-manifold methods should be most effective when there has been significant DR**, and we would expect them to markedly boost recall.

We have therefore demonstrated a dual benefit in using the Finding Pegasus Approach when significant DR has been applied: the contribution to recall from A_{on} will be higher

because the on-manifold AD method is being used in lower-D; and the contribution from A_{off} will also be greater.

5.6. Relationship between A_{on} and A_{off}

Note in general $A_{on} \cap A_{off} \neq \emptyset$ since there might be anomalous points which are poorly represented on the low-D manifold yet are still detectable on it because of high correlation between the features which have been lost in compression and the ones that remain. This notwithstanding, **since A_{off} is a consequence of the manifold construction, whilst A_{on} results from the choice of AD technique used on the manifold, they are likely to represent points with very different sets of features** (as we saw in Section 4.2) especially when DR is significant. Thus, combining on- and off-manifold sets of anomalies as per the Finding Pegasus Approach and Equation 11 will not just maximize recall, but also likely increase diversity of anomalies detected. As we have seen, however, in 5.4, the relative size of the two sets will depend on the scale of the DR applied. For $M \lesssim D$, $|A_{off}| \ll |A_{on}|$ whereas for $M \ll D$, $|A_{off}| \approx |A_{on}|$.

6. Application to MNIST Handwritten Digits

To validate the concepts outlined in this paper, we applied them to an illustrative high-D dataset: MNIST (Deng, 2012). We chose this as we believe our approach has wide applicability, and MNIST is familiar to most researchers. In testing, we attempted to detect images of 8s and 7s from a bulk population of 1s, using on- and off-manifold methods applied to four manifolds (PCA and AE, in both $M \lesssim D$ and $M \ll D$ regimes). AD methods used were PCA or AE reconstruction error (RE), IF, LOF, EE and OCSVM. Methods were tested standalone, and then combined first with RE (our Finding Pegasus approach), and subsequently with IF. Details are given in Appendix G, a summary of findings presented below, and the most significant results, from the $M = 30$ AE manifold, are shown in Table 1.

We found that, regardless of manifold, Isolation Forest (IF) was the most effective on-manifold method for AD recall on a standalone basis. We also observed that for any of the four manifolds, combining an on-manifold AD method with the off-manifold RE method boosted recall. This is a trivial result arising from the definition of recall, however, the mean F1 score also improved, showing that precision was not unduly sacrificed. The best performance was for the $M = 30$ AE manifold where mean Finding Pegasus recall was 84% compared to mean standalone methods of 50%.

We also saw (Table 1) that with the $M = 30$ AE manifold, **our Finding Pegasus approach of combining AD**

Table 1. AD Recall and F1 from testing MNIST with $M = 30$ AE manifold. AD methods tested standalone, then combined with AE reconstruction error (RE, our Finding Pegasus approach) or IF.

AD Method	AE manifold, $M = 30$					
	Stand-alone		with AE RE F. Pegasus		with IF	
	Rec.	F1	Rec.	F1	Rec.	F1
<i>Off Manifold</i>						
AE RE	0.73	0.73	n/a	n/a	n/a	n/a
<i>On Manifold</i>						
IF	0.60	0.60	0.88	0.73	n/a	n/a
LOF	0.18	0.18	0.78	0.56	0.75	0.51
EE	0.59	0.59	0.88	0.74	0.70	0.62
OCSVM	0.41	0.41	0.83	0.65	0.61	0.51
Mean	0.50	0.50	0.84	0.67	0.68	0.55

methods performed 16% better on average than simply combining an on-manifold AD method with the best standalone on-manifold AD method, IF (84% v 68%). In fact, with this manifold, all on-manifold AD methods performed significantly better using the Finding Pegasus approach than by combining with IF.

Considering the types of anomalies found, we observed that when we apply substantial DR, the proportion of 8s detected by reconstruction error (the *Pegasus* type anomalies) markedly increased, and again this was higher when using the AE manifold (88% using AE, $M = 30$, Table 6). This supports our idea that, with high DR, off-manifold methods will be effective at identifying anomalies which do not solely reflect extremes of the bulk data (important as those might be) but which also exhibit novel features (in this case topological) where they are uncorrelated with bulk features.

All these results demonstrate the increased effectiveness with significant DR of our Finding Pegasus approach; and also perhaps indicate that the non-linear AE creates a better manifold from the non-linear dataset than linear PCA.

Finally, we observed (e.g. Fig 10) that even when all the on-manifold methods were combined, there were some anomalies only detectable by the off-manifold method, further illustrating the importance of the Finding Pegasus approach.

7. Summary of Key Concepts

- Unsupervised AD techniques can struggle with high-D data, meaning researchers often choose to work in low-D. DR creates a manifold which is model dependent, and the anomalies detected using it are consequently also model dependent.
- We have reframed the unsupervised AD problem from

the perspective of the lower-D manifold, encouraging thinking about unsupervised AD techniques and anomalies as being either on manifold or off manifold.

- Substantial DR should a) improve the efficacy of unsupervised on-manifold methods and b) increase the number of off-manifold anomalies, $|A_{off}|$.
- However, the number of on-manifold anomalies detected is limited to $|A_d|$, so when DR is high, $|A_{on}| \approx |A_{off}|$ meaning AD relying solely on on-manifold methods will have an effective ceiling on recall.
- Recall will therefore be maximised by combining complementary on- and off-manifold methods (our Finding Pegasus approach) under condition of significant DR.
- Off-manifold anomalies are potentially of a very different character to on-manifold given they are a consequence of manifold construction rather than of the on-manifold detection technique.

We trust this paper’s illustrations and formalism will be of value to a variety of discovery-driven fields of research utilising high-D data – e.g. astronomy, medical imaging, signal processing, financial fraud detection – and will motivate such researchers to consider their application.

Acknowledgements

We thank NOIR Lab, DESI Collaboration and Breakthrough Discuss at whose conferences early versions of this work were presented; and Chris Lintott, Constantina Nicolaou, Tara Tahseen, James Ray, Or Graur, Segev Ben-Zvi, John Suárez-Pérez, Lucy Fortson, Colin Jacobs, Antonella Palmese, Peter Melchior, Kameswara Mantha, Hayley Roberts, Koketso Mohale, Javier Viaña Pérez, and Bruce Bassett for insightful conversation, feedback and encouragement.

RPN has been supported by the STFC UCL Centre for Doctoral Training in Data Intensive Science (grant ST/W00674X/1) and departmental and industry contributions. OL acknowledges STFC Consolidated Grant ST/R000476/1 and visits to All Souls College and the Physics Department, University of Oxford.

References

- Barnett, V. and Lewis, T. Outliers in statistical data, 3rd ed. 1994.
- Bellman, R. Dynamic programming. *Science*, 153(3731): 34–37, 1966.
- Bishop, C. M. *Pattern Recognition and Machine Learning (Information Science and Statistics)*. Springer, 1 edition, 2007. ISBN 0387310738.
- Breunig, M. M., Kriegel, H.-P., Ng, R. T., and Sander, J. Lof: identifying density-based local outliers. *SIGMOD Rec.*, 29(2):93–104, may 2000. ISSN 0163-5808.
- Chollet, F. et al. Keras. <https://keras.io>, 2015.
- Delon, J. The curse of dimensionality, 2017.
- Deng, L. The mnist database of handwritten digit images for machine learning research. *IEEE Signal Processing Magazine*, 29(6):141–142, 2012.
- DESI Collaboration, Aghamousa, A., Aguilar, J., Ahlen, S., Alam, S., Allen, L. E., Allende Prieto, C., Annis, J., Bailey, S., Balland, C., Ballester, O., Baltay, C., Beaufore, L., Bebek, C., and Beers, T. C. a. The DESI Experiment Part I: Science, Targeting, and Survey Design. *arXiv e-prints*, 2016.
- Edgeworth, F. On discordant observations. *The london, Edinburgh, and Dublin Philosophical Magazine and Journal of Science*, 23(5):364–375, 1887.
- Géron, A. *Hands-On Machine Learning with Scikit-Learn, Keras and TensorFlow*. O’Reilly, 2023. ISBN 978-1-098-12597-4.

- Goodfellow, I. J., Bengio, Y., and Courville, A. *Deep Learning*. MIT Press, Cambridge, MA, USA, 2016.
- Han, S., Hu, X., Huang, H., Jiang, M., and Zhao, Y. Ad-bench: Anomaly detection benchmark, 2022.
- Kingma, D. P. and Welling, M. Auto-encoding variational bayes, 2022. URL <https://arxiv.org/abs/1312.6114>.
- Kramer, M. A. Nonlinear principal component analysis using autoassociative neural networks. *AIChE Journal*, 37(2):233–243, February 1991. doi: 10.1002/aic.690370209.
- Langley, P. Crafting papers on machine learning. In Langley, P. (ed.), *Proceedings of the 17th International Conference on Machine Learning (ICML 2000)*, pp. 1207–1216, Stanford, CA, 2000. Morgan Kaufmann.
- Liu, F. T., Ting, K. M., and Zhou, Z.-H. Isolation forest. In *2008 Eighth IEEE International Conference on Data Mining*, pp. 413–422, 2008. doi: 10.1109/ICDM.2008.17.
- Pedregosa, F., Varoquaux, G., Gramfort, A., Michel, V., Thirion, B., Grisel, O., Blondel, M., Prettenhofer, P., Weiss, R., Dubourg, V., Vanderplas, J., Passos, A., Cournapeau, D., Brucher, M., Perrot, M., and Duchesnay, E. Scikit-learn: Machine learning in Python. *Journal of Machine Learning Research*, 12:2825–2830, 2011.
- Portillo, S. K. N., Parejko, J. K., Vergara, J. R., and Connolly, A. J. Dimensionality reduction of SDSS spectra with variational autoencoders. *The Astronomical Journal*, 160(1):45, jun 2020. doi: 10.3847/1538-3881/ab9644.
- Ramaswamy, S., Rastogi, R., and Shim, K. Efficient algorithms for mining outliers from large data sets. In *Proceedings of the 2000 ACM SIGMOD International Conference on Management of Data, SIGMOD '00*, pp. 427–438, New York, NY, USA, 2000. Association for Computing Machinery. ISBN 1581132174.
- Rousseeuw, P. and Driessen, K. A fast algorithm for the minimum covariance determinant estimator. *Technometrics*, 41(6):212–223, August 1999. doi: 10.1080/00401706.1999.10485670.
- Roweis, S. T. and Saul, L. K. Nonlinear dimensionality reduction by locally linear embedding. *Science*, 290(5500):2323–2326, 2000. doi: 10.1126/science.290.5500.2323.
- Ruff, L., Kauffmann, J. R., Vandermeulen, R. A., Montavon, G., Samek, W., Kloft, M., Dietterich, T. G., and Müller, K. A unifying review of deep and shallow anomaly detection. *CoRR*, abs/2009.11732, 2020.
- Schölkopf, B., Williamson, R., Smola, A., Shawe-Taylor, J., and Platt, J. Support vector method for novelty detection. *NIPS*, 12:582–588, January 1999.
- van der Maaten, L. and Hinton, G. E. Visualizing data using t-sne. *Journal of Machine Learning Research*, 9:2579–2605, 2008.
- Wolpert, D. The lack of a priori distinctions between learning algorithms. *Neural Computation*, pp. 1341–1390, 1996.
- Yip, C. W., Connolly, A. J., Berk, D. E. V., Ma, Z., Friedman, J. A., SubbaRao, M., Szalay, A. S., Richards, G. T., Hall, P. B., Schneider, D. P., Hopkins, A. M., Trump, J., and Brinkmann, J. Spectral classification of quasars in the sloan digital sky survey: Eigenspectra, redshift, and luminosity effects. *The Astronomical Journal*, 128(6):2603–2630, dec 2004a. doi: 10.1086/425626.
- Yip, C. W., Connolly, A. J., Berk, D. E. V., Ma, Z., Friedman, J. A., SubbaRao, M., Szalay, A. S., Richards, G. T., Hall, P. B., Schneider, D. P., Hopkins, A. M., Trump, J., and Brinkmann, J. Spectral classification of quasars in the sloan digital sky survey: Eigenspectra, redshift, and luminosity effects. *The Astronomical Journal*, 128(6):2603, dec 2004b. doi: 10.1086/425626.
- Zhao, Y., Nasrullah, Z., and Li, Z. Pyod: A python toolbox for scalable outlier detection. *Journal of Machine Learning Research*, 20(96):1–7, 2019.

A. Standard Metrics

Where we have a good expectation of the incidence of anomalies we are likely to find within a sample, we can measure an AD method’s effectiveness in terms of standard metrics of recall and precision as follows:

$$Recall = \frac{|TP|}{|TP| + |FN|} \quad (12)$$

$$Precision = \frac{|TP|}{|TP| + |FP|} \quad (13)$$

where TP are True Positives, FN are False Negatives, and FP are False Positives (and TN would be true negatives).

The F1 score is used as a way of combining recall and precision into a single metric and is often viewed as a measure of the all-round performance of an algorithm. It is defined from the harmonic mean of recall and precision as follows:

$$F1 = 2 \times \frac{Recall \times Precision}{Recall + Precision} \quad (14)$$

B. The Curse of Dimensionality

For many domains of research where the raw data representation of observations is in high-D, that representation is a consequence of how the data are collected rather than reflecting any underlying properties of the object. In our astronomy example, DESI spectra of target objects are captured across approximately 7800 small wavelength intervals called spectral channels or bins. High-D data like this is more onerous to work with computationally, and means we are likely to be afflicted by the Curse of Dimensionality.

First coined by (Bellman, 1966), the Curse of Dimensionality refers to how our intuition into data behaviour begins to fail as we move beyond three dimensions. Two examples which are of particular importance in AD are the way that notions of **distance** and **concentration** are affected in high-D.

B.1. Distance Metrics in high-D

As the number of dimensions in a data representation rises, the volume of space contained in the representation also rises. As a consequence, in high-D data points become increasingly sparse and distant from one another. E.g. if \mathbf{x} and \mathbf{y} are two independent variables, uniformly distributed on $[0, 1]^D$, where D is the dimensionality of the space, then the mean square distance between them $\|\mathbf{x} - \mathbf{y}\|^2$ is given by (Delon, 2017):

$$\mathbb{E}[\|\mathbf{x} - \mathbf{y}\|^2] = D/6 \quad (15)$$

and the standard deviation by:

$$Std[\|\mathbf{x} - \mathbf{y}\|^2] \approx 0.2\sqrt{D} \quad (16)$$

i.e. as the dimensionality increases, points get further apart but are relatively more tightly spread. As a result of this, the concept of nearest neighbours, which is fundamental to many AD techniques, starts to fail.

B.2. Concentration in high-D

As well as being further away from each other as dimensionality increases, points also tend to be closer to the boundary of the space. A simple way to think of this is that in a high-D space – i.e. one where the data is represented by many features – it is highly likely that at least one of these features will have an extreme value. Gaussian distributions also behave differently in high dimension to our experience from low (one or two) dimensional representations. E.g. for a multivariate Gaussian of D parameters, the distance from the centre at which the maximum concentration of points is found migrates away from zero and is found instead at $r = \sqrt{D - 1}$ (Delon, 2017).

C. Schematic Summary of On- and Off-Manifold Anomalies when Dimensionality Reduction has been performed

A schematic showing relationship between on- and off-manifold anomalies when performing AD after dimensionality reduction is shown in Fig. 3.

D. Commonly Used Unsupervised Machine Learning Models

D.1. DR

- *Local Linear Embedding* (Roweis & Saul, 2000): Looks at how each training instance linearly relates to k nearest neighbours and then finds a low-D representation which best preserves those local relationships.
- *t-SNE* (van der Maaten & Hinton, 2008): Reduces dimensionality of the dataset while keeping similar instances close and dissimilar ones further apart. This method is widely used for the visualization in 2D or 3D of clusters existing in much higher dimensional space.
- *Autoencoder (AE)* (Kramer, 1991): A neural network which learns efficient codings of unlabelled data by compressing them into low-D. An autoencoder consists of encoder and decoder layers with a latent layer in-between. It is the size of this latent layer which sets

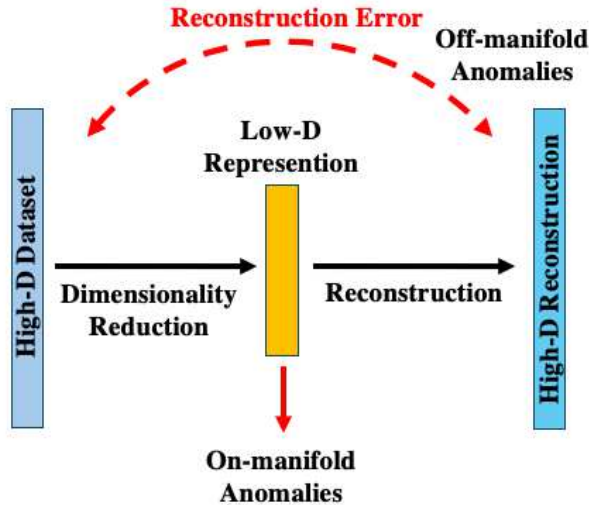


Figure 3. Schematic showing relationship between on- and off-manifold anomalies when performing AD after dimensionality reduction.

the dimensionality to which the data is compressed. The low-D representation created by the encoder is known as the latent space. The decoder layers then attempt to reconstruct the input signal. Activation functions between layers are typically non-linear. In the special case where the activation functions are linear and there are only one encoder and decoder layers, then the autoencoder behaves like PCA.

- *Variational Autoencoder (VAE)* (Kingma & Welling, 2022): A neural network similar to an autoencoder, but where the input is now mapped onto a multivariate Gaussian distribution, characterised by a set of means and standard deviations. Again, the level of compression of the original data is set by the size of the latent layer. VAEs are probabilistic in nature and are often preferred over autoencoders for their generative properties – new points can be sampled from the latent distributions and run through the trained decoder.

D.2. AD

- *Gaussian Mixture Model (GMM)*, e.g. Géron 2023): A probabilistic model which makes the assumption that the dataset comprises points which were samples from a mixture of multiple Gaussian distributions with unknown parameters.
- *K-Nearest Neighbours (KNN)*, Ramaswamy et al. 2000): Assigns an anomaly score to the data instance based on its distance to its k -th nearest neighbour.
- *Local Outlier Factor (LOF)*, Breunig et al. 2000): The algorithm compares the density of points around a

given point to the density around the neighbouring points. A point is deemed an anomaly if it is more isolated (in a region of relative under-density) than its k nearest neighbours.

- *Elliptic Envelope* (Rousseeuw & Driessen 1999): the model assumes the data is Gaussian and learns an ellipse; outliers are outside this ellipse.
- *One-Class Support Vector Machine* (One-Class SVM, Schölkopf et al. 1999): the model attempts to learn a decision boundary which encloses the target class in feature space, thereby characterising the normal data.
- *Isolation Forest* (IF, Liu et al. 2008): Features are randomly sub-sampled and recursively partitioned into a tree structure until all data points are isolated. Because anomalies are expected to be ‘few and different’ they should be found closer to the root of the tree. IF is still affected by sparsity issues in high-D representations, hence a sub-space of features is often chosen, typically by ranking them by kurtosis, and these are used to construct the isolation forest. Kurtosis is sensitive to anomalies and hence a good selection criterion. But this sub-space is simply a low-D hyperplane in the original high-D space. Hence, Isolation Forest with kurtosis is simply another example of an on-manifold approach.

E. Formal Framework for AD in High-D data – Further Considerations

A schematic overview of the framework described in Section 5 is provided in Fig. 2. Further points of consideration arising from our framework are provided in the sections below.

E.1. Undetectable Anomalies in Raw Data Representation

We note that we could further decompose the set of normal points, N , as follows:

$$N = N^N \cup N^A, \quad N^N \cap N^A = \emptyset \quad (17)$$

i.e. of the points we would observe as being normal, some, N^N , are indeed normal, whilst some, N^A , are in fact anomalies, but are undetectable even in the raw D -dimensional representation. The features which make these points diverge from normality, along with any highly correlated proxies, are not contained within the raw representation, and hence it simply would not be possible to detect them, irrespective of time, tools, or expertise. Since we cannot distinguish these points using the full information at our disposal, we have no choice but to treat these points as normal.

E.2. Detectability in Reduced Dimensionality

In the native dimensionality, D , it is natural to think of detectability of anomalies in terms of an expert manually sifting through an entire dataset, taking as long as needed to painstakingly inspect each instance for oddities which would indicate it to be anomalous. They would use visual inspection and any other tool they wished to perform this task. (The ‘painstaking’ aspect of this process is, of course, one of the reasons why we choose to use machine learning for AD in the first place, since manual approaches are not inherently scalable.) If an instance is identifiable by an expert using such methods then we consider it a detectable anomaly, and if not then it is an undetectable anomaly.

Especially where non-linear methods have been used to create the low-D manifold, however, an individual who was expert in interpreting data instances in the native dimensionality is unlikely to be familiar with their representation in lower dimension. We therefore extend our definition of detectability to reduced dimensionality by imagining a hypothetical expert who has adequate time to become fully acquainted with the low-D representation and is able to develop and apply methods and tools which could be used to identify anomalies within it. We note that some of these might well be the very machine learning methods described in Section 3.3.

Accordingly, we can define an anomalous point as being detectable in the low-D representation if our hypothetical expert, with access to sufficient time and tools, would be able to find it. Similarly, where we have normal points which are labeled anomalous in the low-D representation, it is because our hypothetical expert would identify them as such.

E.3. Relaxing the Requirement for a Good AD Model for a Particular Manifold

Reliance on a good AD method will be mitigated where DR has been significant, since this will increase the balance of total anomalies towards off-manifold anomalies, and it should also make the on-manifold unsupervised AD methods more effective. This points to a way of further optimising the anomalies detected.

Consider that for a given manifold of dimension M we use two different models, mod_1 and mod_2 , then these will detect sets of anomalies $A_{mod_1} = A_{on_1}$ and $A_{mod_2} = A_{on_2}$. In general, $A_{mod_1} \cap A_{mod_2} \neq \emptyset$ and if we have not chosen the models to be ‘good’ models as described in Section 5.5.1, then neither A_{on_1} nor A_{on_2} are required or expected to be approximately equal to A_d .

The off-manifold points are, as noted previously, a consequence of manifold construction and so will be the same in both cases.

We can extend this to use a set of models working on the M -dimensional manifold, $\mathbb{S} = \{model_1, model_2 \dots model_n\}$ to form the superset of on-manifold anomalies:

$$A_{on,\mathbb{S}} = A_{on,1} \cup A_{on,2} \cup \dots \cup A_{on,n} \quad (18)$$

If we pick models which use different methodologies to detect outliers then we might expect that even for small n we might be able to say $A_{on,\mathbb{S}} \approx A_d$, i.e. the set of models will perform as well as a single ‘good’ model.

Although it might seem obvious to suggest combining on-manifold methods to boost recall, the key point here is that there is no requirement to first search for ‘good’ models, and that especially where $M \ll D$, and D is high, then there may not be easy to find a single model which meets our definition of ‘good’. Rather, we would suggest using combinations of models that employ different algorithms.

Note, however, that even with multiple models, our maximum recall will be limited to A_d which will be problematic where there has been significant DR. In order to boost recall when $M \ll D$ further we must still use the Finding Pegasus approach so that we also include anomalous points which are poorly represented in the low-D representation.

E.4. The Importance of the Choice of Manifold Model

In contrast to the previous section, we should note it is still important to build a good manifold, i.e. one for which the majority of points in the dataset are well represented, thereby satisfying the manifold hypothesis and in so doing, minimizing N_- and N_d . Without this constraint, true anomalies could be swamped by false positive normal points rendering expert review of these points much more onerous and perhaps even impossible. In addition, a good manifold means that off-manifold anomalies are by definition instances which differ significantly different from the feature set which characterize the bulk of the population. Where these features encode physical features, it would suggest that off-manifold anomalies could encompass instances displaying new physics (as discussed in Section 4).

E.5. Reconstruction from Low-D

We note that reconstruction from the reduced dimensional representation is not possible from some commonly used DR techniques, and so for AD purposes care should be taken in the choice of method to pick one which will allow this.

E.6. Achieving High Recall

It also follows from Equations 6, 9 and 10 that $A_{off} = A_- \approx A_u$, i.e. that off-manifold anomalies, detectable through reconstruction error, will be similar to the set of

anomalies which are no-longer distinguishable from normal points on the M -dimensional manifold. Hence:

$$A_{on} \cup A_{off} \approx A_d \cup A_u = A' \quad (19)$$

Hence, we have shown that where we have a good model applied to a well constructed manifold incorporating a high level of DR, using the Finding Pegasus approach (i.e. combining complementary on- and off-manifold AD techniques) might boost recall sufficiently to enable us to identify a large proportion of the anomalies in X .

F. Applying the Formal Framework

We now demonstrate how the formal framework described in Section 5 might be used in practice. First we apply the framework to the idealized dataset depicted in the Finding Pegasus illustration. Then we shall show how it might be used to derive generalised expressions for precision and recall.

F.1. Analysis of Finding Pegasus Illustration

F.1.1. OVERVIEW

For the purposes of this analysis, and reflecting the discussion in Section 4.1, we shall include *two* Pegasus points, one with magical (i.e. weightless) wings and one with heavy wings. A summary of how these points would be represented using our framework is shown in Table 2.

The first two columns of the table reflect how well or poorly the anomalous points are represented on the lower-dimension manifold. The third and fourth columns indicate whether the anomalous points are detectable or undetectable on the lower-dimensional manifold.

We note that anomalous points which are poorly represented on the manifold are off-manifold anomalies by definition and are given by the second column in Table 2.

Making the assumption that we can find a ‘good’ model as described in Section 5.5.1 to search for anomalies on the low-D manifold we have created (2D in this example) then we would expect to find most of the detectable anomalies. Hence the on-manifold anomalies will be the set of points appearing in the third column.

F.1.2. Eohippus AND Sampson

Taking *Eohippus* and *Sampson* first, we see both points are categorized as being well represented on the manifold and also being detectable on the manifold. Because of the latter, they will be part of the set of on-manifold anomalies.

Table 2. Finding Pegasus illustration categorized according to framework in Section 5

	$\in A_+$	$\in A_-$	$\in A_d$	$\in A_u$
<i>Eohippus</i>	✓		✓	
<i>Sampson</i>	✓		✓	
<i>Pegasus</i>				
- magical wings		✓		✓
- heavy wings		✓	✓	

F.1.3. Pegasus_m AND Pegasus_h

Pegasus with magical wings, *Pegasus_m*, is poorly represented on the manifold, hence an off-manifold anomaly by definition. Because the wing feature had no correlation with the two retained features of height and weight it was projected down into the centre of the distribution of normal horse points. Hence *Pegasus_m* is unlikely to be detectable on the manifold.

Pegasus with heavy wings, *Pegasus_h*, is also poorly represented on the manifold, hence an off-manifold anomaly by definition. Now though, its heavy wings will mean it is no longer projected into the centre of the distribution of normal horse points but will be found in a lower density region representing horses with abnormally high weight. Thus *Pegasus_h* should be detectable on the manifold.

In summary then we will have:

$$A_{on} = \{Eohippus, Sampson, Pegasus_h\} \quad (20)$$

and

$$A_{off} = \{Pegasus_m, Pegasus_h\} \quad (21)$$

We can therefore see that *Pegasus_h* will be an element of the sets of both on- and off-manifold anomalies. Consequently, and as discussed in Section 5.6:

$$A_{on} \cap A_{off} \neq \emptyset \quad (22)$$

F.2. Derivation of Expressions for Recall and Precision

We now apply the formal framework to derive expressions for recall and precision metrics as introduced in Section 2 and defined in equations 12 and 13 respectively.

F.2.1. ON MANIFOLD

For on-manifold anomalies we assume we are using a good model with $M \ll D$ on a well constructed manifold as previously defined and so can say, knowing $A_{on}^* \approx A_d \cup N_d$ that:

$$TP_{on} = A_{mod} \approx A_d \quad (23)$$

and

$$FP_{on} = N_{mod} \approx N_d \quad (24)$$

Since $TP_{on} \cup FN_{on} = A'$, i.e. the union of the sets of true positives and false negatives must equal the entire set of anomalies, then using Equation 4 we can say the anomalous points not captured must be:

$$FN_{on} \approx A_u \quad (25)$$

Thence:

$$Recall_{on} \approx \frac{|A_d|}{|A_d| + |A_u|} = \frac{|A_d|}{|A'|} \quad (26)$$

$$Precision_{on} \approx \frac{|A_d|}{|A_d| + |N_d|} \quad (27)$$

From Equation 26 we can see that recall will be limited by $|A_d|$ if we are only using on-manifold methods. And from Equation 27 we can see that a well-constructed manifold which minimises N_d will maximise precision.

F.2.2. OFF MANIFOLD

For off-manifold anomalies we can say, following the arguments in Section 5.5.2, and noting that False Negatives will simply be anomalous points not captured using this method:

$$TP_{off} = A_- \quad (28)$$

$$FP_{off} = N_- \quad (29)$$

$$FN_{off} = A_+ \quad (30)$$

Hence we can say:

$$Recall_{off} = \frac{|A_-|}{|A_-| + |A_+|} = \frac{|A_-|}{|A'|} \quad (31)$$

$$Precision_{off} = \frac{|A_-|}{|A_-| + |N_-|} \quad (32)$$

From Equation 32 we can see that a well constructed manifold which captures most of the normal points and minimizes N_- will maximize the precision of off-manifold AD.

Hence, precision for both on- and off-manifold methods are maximized by building a good manifold.

F.2.3. FINDING PEGASUS APPROACH

We now combine on- and off-manifold methods to determine precision and recall for the Finding Pegasus approach. First let us define the associated metrics TP_f , FP_f and FN_f . From Equations 23 and 28 and using Equation 19 we can see:

$$TP_f \approx A_d \cup A_- \approx A_d \cup A_u = A' \quad (33)$$

It follows immediately that

$$FN_f \approx \emptyset \quad (34)$$

And from Equations 24 and 29:

$$FP_f \approx N_d \cup N_- \quad (35)$$

Hence:

$$Recall_f \approx \frac{|A'|}{|A'| + |\emptyset|} = 1 \quad (36)$$

i.e. recall for this method will approach 100% when we have a good AD method applied to a well constructed manifold as previously implied by Eqn 19.

Similarly we can write:

$$Precision_f \approx \frac{|A'|}{|A'| + |N_d \cup N_-|} \quad (37)$$

If we have maximised precision of both on- and off-manifold anomalies, by minimising $|N_d|$ and $|N_-|$ then we will have also maximised precision overall. Hence, the Finding Pegasus approach should deliver maximum recall without undue penalty to precision.

G. Application of Finding Pegasus Approach to MNIST data

G.1. Choice of Dataset

The MNIST (modified National Institute of Standards and Technology, [Deng, 2012](#)) dataset comprises 60,000 training images and 10,000 test images of handwritten digits of the numbers 0 to 9 in roughly equal quantities, along with corresponding sets of labels. These black and white digits are size normalized to 28x28 pixels giving the dimensionality, D , of each flattened image vector as 784, high enough to be able to test the Finding Pegasus Approach. Whilst

Table 3. Summary of AD testing on MNIST Handwritten Digits using a variety of on-manifold methods in conjunction with PCA manifolds generated at two different levels of DR, first standalone and then combined with PCA Reconstruction Error (the Finding Pegasus Approach) and Isolation Forest methods in turn.

AD METHOD	$D = 784$						PCA manifold, $M = 245$						PCA manifold, $M = 84$					
	Standalone		with PCA RE		with IF		Standalone		with PCA RE		with IF		Standalone		with PCA RE		with IF	
	Rec.	F1	F. Pegasus		Rec.	F1	Rec.	F1	Rec.	F1	F. Pegasus		Rec.	F1	Rec.	F1	Rec.	F1
<i>Off Manifold</i>																		
Reconstruction Error	0.53	0.53	n/a	n/a	n/a	n/a	0.65	0.65	n/a	n/a	n/a	n/a	0.65	0.65	n/a	n/a	n/a	n/a
<i>On Manifold</i>																		
Isolation Forest	0.63	0.63	0.70	0.61	n/a	n/a	0.67	0.67	0.77	0.70	n/a	n/a	0.67	0.67	0.77	0.70	n/a	n/a
LOF	0.29	0.29	0.71	0.52	0.76	0.56	0.25	0.25	0.77	0.56	0.79	0.57	0.25	0.25	0.77	0.56	0.79	0.57
Ellipticenvelope	0.58	0.58	0.72	0.57	0.77	0.62	0.37	0.37	0.75	0.56	0.73	0.55	0.37	0.37	0.75	0.56	0.73	0.55
One-Class SVM	0.60	0.59	0.72	0.60	0.73	0.63	0.56	0.55	0.77	0.65	0.73	0.63	0.56	0.55	0.77	0.65	0.73	0.63
Mean Recall/F1	0.53	0.52	0.71	0.58	0.75	0.61	0.50	0.50	0.76	0.62	0.75	0.59	0.50	0.50	0.76	0.62	0.75	0.59

MNIST might often be regarded as an introductory dataset for supervised classification purposes, it still contains much subtlety which captures well the issues being faced in unsupervised AD in high-D data.

For the purposes of this study we worked with a subset of the test data. We chose the number 1s (comprising approximately 6,700 data points) as the bulk data (the normal points) and contaminated it with anomalies consisting 120 points ($\approx 2\%$) of the 7s dataset to represent an extreme version of the bulk topology; and 120 points ($\approx 2\%$) of the 8s dataset to introduce a class of anomalies with a very different topology, in this case consisting of two conjoined loops. In the parlance of this paper, the 7s might be considered anomalies of the *Eohippus* or *Sampson* type; whereas the 8s could be regarded as anomalies of the *Pegasus* type. Examples of the MNIST handwritten digits used in this work are shown below in Figs. 4, 5 and 6.

Although 7s and 8s are the anomalies we are principally trying to detect, it is worth noting that even within the 1s dataset there are a minority which deviate from the basic form of a single thin vertical line. In particular, there are more complex ‘peaked’ forms (made up of two thin lines: / + |) and ‘peak-and-foot’ forms (made up of three thin lines: / + | + -) which in different contexts might also be viewed as anomalous. We did not attempt to quantify these instances separately here as to do so would require performing a sub-classification of the MNIST 1s dataset, which would have been subjective and not the purpose of this paper.

We note also that we are not seeking to present here the state of the art regarding AD within this dataset, but merely to demonstrate with data how the methods discussed in this paper might be beneficial in practice.

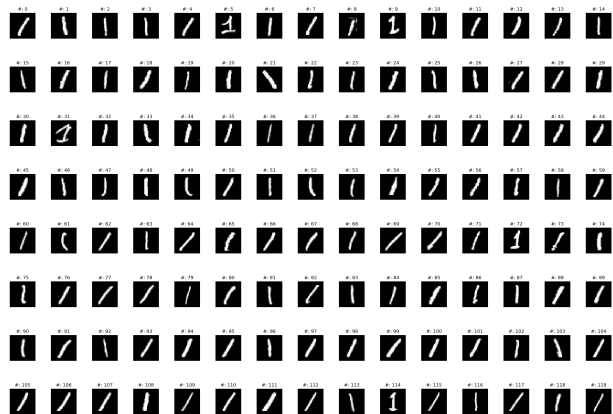


Figure 4. Sample of 1s from MNIST handwritten digits dataset representing ‘normal’ points.

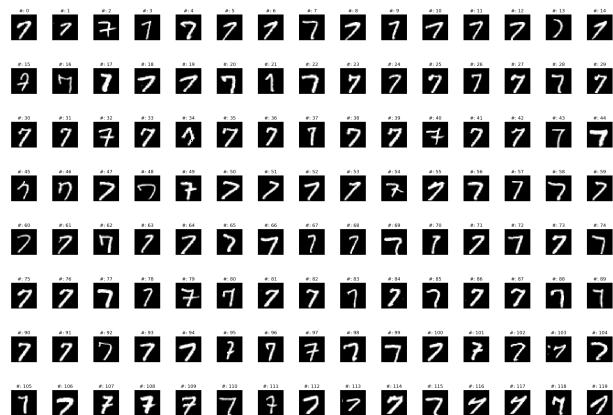


Figure 5. 7s ‘anomalies’ from MNIST handwritten digits dataset representing extreme forms of the bulk topology - *Eohippus* and *Sampson* points.

Table 4. Summary of AD testing on MNIST Handwritten Digits using a variety of on-manifold methods in conjunction with AE manifolds generated at two different levels of DR, first standalone and then combined with AE Reconstruction Error (the Finding Pegasus Approach) and Isolation Forest methods in turn.

AD METHOD	AE manifold, $M = 245$						AE manifold, $M = 30$					
	Standalone		with AE RE		with IF		Standalone		with AE RE		with IF	
	Rec.	F1	F. Pegasus		Rec.	F1	Rec.	F1	F. Pegasus		Rec.	F1
<i>Off Manifold</i>												
Reconstruction Error	0.45	0.45	n/a	n/a	n/a	n/a	0.73	0.73	n/a	n/a	n/a	n/a
<i>On Manifold</i>												
Isolation Forest	0.67	0.67	0.71	0.58	n/a	n/a	0.60	0.60	0.88	0.73	n/a	n/a
LOF	0.41	0.41	0.70	0.50	0.85	0.64	0.18	0.18	0.78	0.56	0.75	0.51
Ellipticenvelope	0.45	0.45	0.73	0.55	0.86	0.66	0.59	0.59	0.88	0.74	0.70	0.62
One-Class SVM	0.60	0.60	0.66	0.53	0.75	0.67	0.41	0.41	0.83	0.65	0.61	0.51
Mean Recall/F1	0.50	0.52	0.76	0.54	0.75	0.66	0.50	0.50	0.84	0.67	0.68	0.55

Table 5. Summary of AD testing on MNIST Handwritten Digits showing the number of off-manifold and on-manifold anomalies detected at two different levels of DR using PCA manifolds. 7s can be considered *Eohippus*-type anomalies.

AD METHOD	PCA manifold, $M = 245$				PCA manifold, $M = 84$			
	7s		8s		7s		8s	
	detected	Recall	detected	Recall	detected	Recall	detected	Recall
<i>Off Manifold</i>								
Reconstruction Error	86	0.72	41	0.34	89	0.74	67	0.56
<i>On Manifold</i>								
Isolation Forest	79	0.66	72	0.60	71	0.59	89	0.74
LOF	28	0.23	42	0.35	24	0.20	36	0.30
Ellipticenvelope	85	0.71	55	0.46	36	0.30	53	0.44
One-Class SVM	67	0.56	78	0.65	62	0.52	72	0.60
Mean On Manifold	65	0.54	62	0.51	48	0.40	63	0.52

Table 6. Summary of AD testing on MNIST Handwritten Digits showing the number of off-manifold and on-manifold anomalies detected at two different levels of DR using AE manifolds. 8s can be considered *Pegasus*-type anomalies.

AD METHOD	AE manifold, $M = 245$				AE manifold, $M = 30$			
	7s		8s		7s		8s	
	detected	Recall	detected	Recall	detected	Recall	detected	Recall
<i>Off Manifold</i>								
Reconstruction Error	34	0.28	73	0.61	70	0.58	105	0.88
<i>On Manifold</i>								
Isolation Forest	58	0.48	102	0.85	64	0.53	79	0.66
LOF	48	0.40	51	0.43	24	0.20	18	0.15
Ellipticenvelope	85	0.71	24	0.20	72	0.60	70	0.58
One-Class SVM	62	0.52	82	0.68	50	0.42	49	0.41
Mean On Manifold	63	0.53	65	0.54	43	0.44	54	0.45

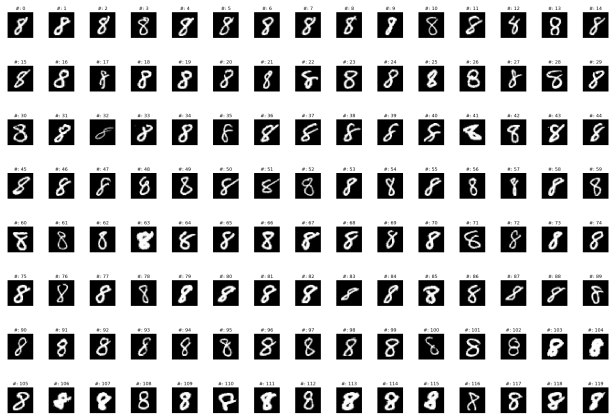


Figure 6. 8s ‘anomalies’ from MNIST handwritten digits dataset representing a radically different topology - *Pegasus* points.

G.2. Summary of Testing Performed

In order to test the ideas of this paper, we used both linear and non-linear methods to reduce the dimensionality of the ≈ 7000 data points comprising the dataset described above and build lower-dimensional manifolds from them. The methods used were PCA projection (linear) and AE manifold learning (non-linear). For each, we chose two levels of DR to roughly correspond to the $M \lesssim D$ and $M \ll D$ regimes introduced in Section 5.4 and which satisfied the manifold hypothesis of achieving a good lower-dimensional representation of the dataset. More detail on manifold construction is given in Section G.3 below. These resulting lower-dimensional manifolds were then used for off-manifold and on-manifold AD.

Off-manifold AD was performed by measuring the MSE between a data point’s original representation and the reconstruction from its manifold representation. Anomalies were defined as the least-well represented 240 points detected, i.e. those with the highest reconstruction error.

On-manifold AD was performed using the Scikit-learn Python implementation of four different commonly used techniques: Local Outlier Factor, Isolation Forest, One-Class Support Vector Machine and EllipticEnvelope. In each case anomalies were defined as the 240 most outlying points using whichever metric was implicit to the method.

For the sets of anomalies detected using these different methods, we calculated recall, precision and F1 metrics, as previously defined, with detected 7s and 8s being regarded as True Positives and all detected 1s being treated as False Positives, regardless of whether we thought them to be unusual forms of the kind mentioned above.

For each manifold, we then looked at the recall and precision of the unions of sets of anomalies from a) the off-manifold reconstruction error approach combined with

each on-manifold approach in turn – i.e. the Finding Pegasus Approach; and b) Isolation Forest combined with each of the other on-manifold detection methods in turn. This latter was done to see whether combining two on-manifold methods would give as good an outcome as our paper’s proposed approach of combining complementary methods. Isolation Forest was chosen to pair with as it gave the best standalone results of the on-manifold methods for both AE and PCA manifolds. Results from manifold testing are shown in Tables 3 and 4.

We also examined the composition of anomalies detected by on- and off-manifold methods across all four of the manifolds we constructed. e.g. the anomalies detected as the least well reconstructed points on the PCA manifold at $M = 84$ is shown in Fig. 9. Of the 240 worst-fitting points 89 are 7s and 67 are 8s. We note also how the 1s which have been identified look different to a typical single vertical line. The mix of 7s and 8s detected for each method with each manifold is given in Tables 5 and 6.

Further details on manifold construction and visualisation of the data is given in the next section.

G.3. Manifold Construction and Data Visualisation

G.3.1. PCA MANIFOLDS

PCA manifolds were built using the Scikit-Learn implementation of PCA. The dimensionalities of the PCA manifolds were $M=245$ ($M \lesssim D$, c.f. $D=784$) with a data variance explained by the PCA decomposition of 99.5%; and $M=84$ (putting it somewhere between the two regimes but closer to $M \ll D$) explaining 95% of the data variance. This was deemed to be a reasonable level at which we could assume the manifold hypothesis still held.

We calculated the MSE between the original representation of each data point and its reconstruction from the PCA representation. Those which were worst represented had a higher MSE. The worst 240 points were assumed to be anomalies. The results for the $M = 84$ manifold are shown in Fig. 11 with anomalies to the right of the dashed green line.

If PCA reconstruction error were a perfect method of determining anomalies (these being defined as images of digits classified as 7s and 8s) then we would expect to see all of these to the right of the green line. The anomalies actually detected for the PCA manifold $M = 84$ are shown in Fig. 9. Of the 240 worst-fitting points 89 are 7s and 67 are 8s. We note also how the 1s which have been identified look different to a typical single vertical line.

We then built a 2D representation of the PCA manifold using t-SNE to see a representation of the distribution of the points upon it. For the $M = 84$ manifold this is shown in

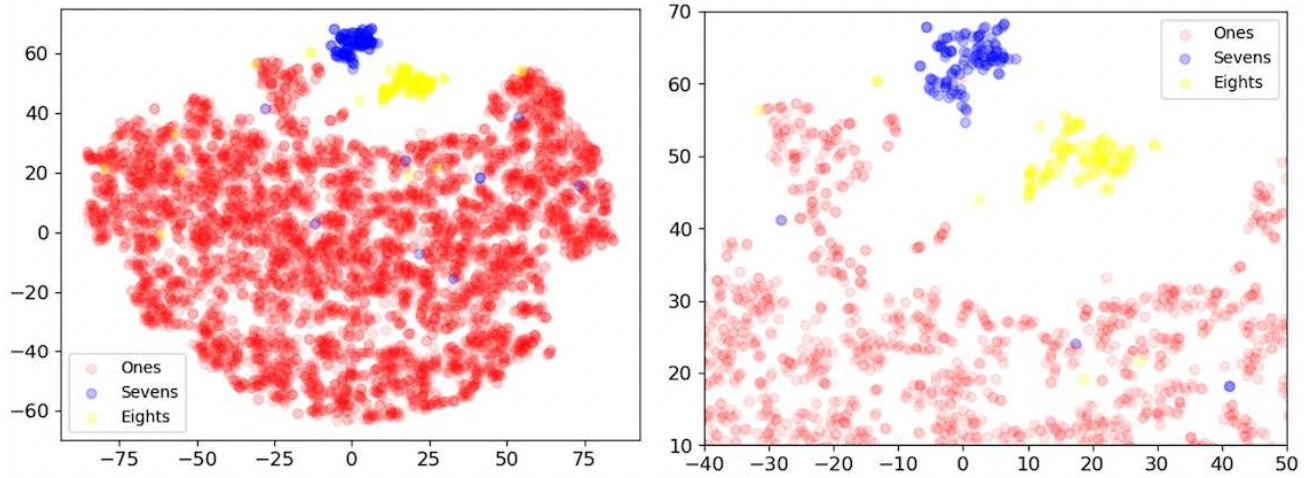


Figure 7. t-SNE 2D representation of distribution of dataset points upon the PCA manifold $M = 84$ with 1s shown in red, 7s in blue and 8s in yellow. We can see clearly the two “islands” where most of the 7s and 8s reside. This is shown zoomed in in the figure on the right.

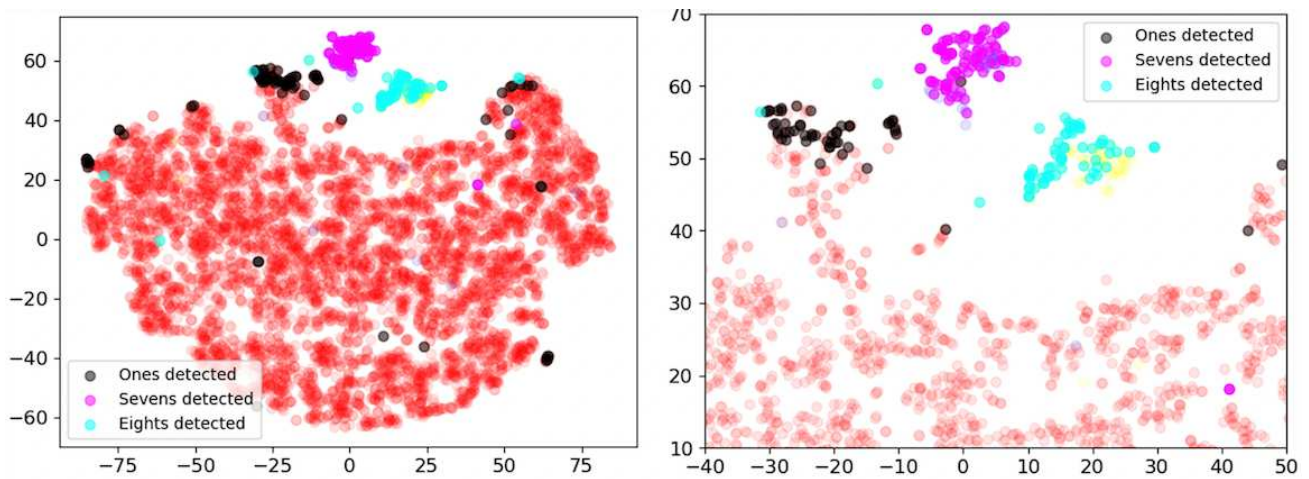


Figure 8. t-SNE 2D representation of distribution of dataset points upon the PCA manifold $M = 84$ with points detected as anomalies by off-manifold reconstruction error highlighted. Detected 7s are shown in magenta, detected 8s in cyan, and the detected 1s (false positive anomalies) are shown in black. The subfigure to the right shows a zoomed-in view of this. We can see immediately that the reconstruction error approach is doing a decent job of identifying the “islands” of both 7s and 8s.

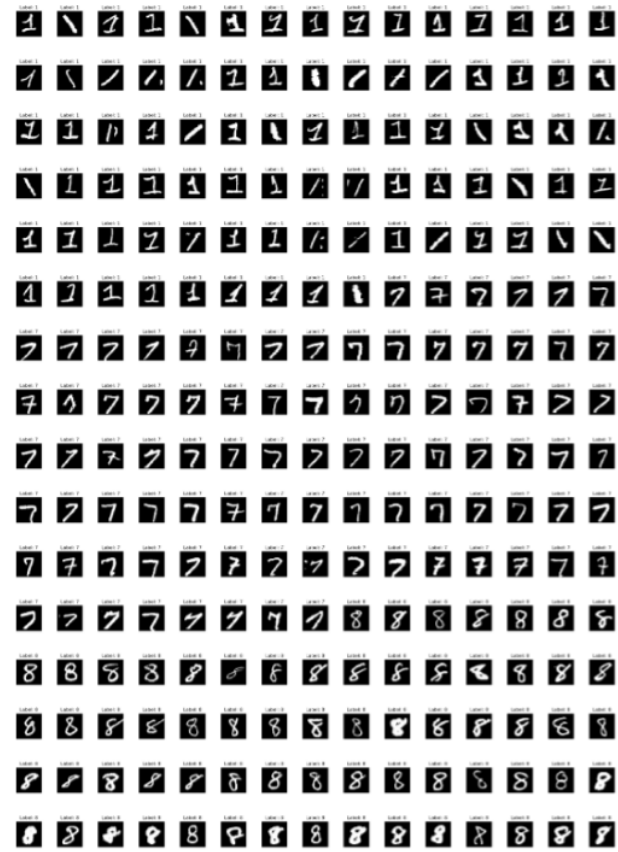


Figure 9. ‘Anomalies’ detected from MNIST handwritten digits dataset using reconstruction error from PCA manifold at $M = 84$

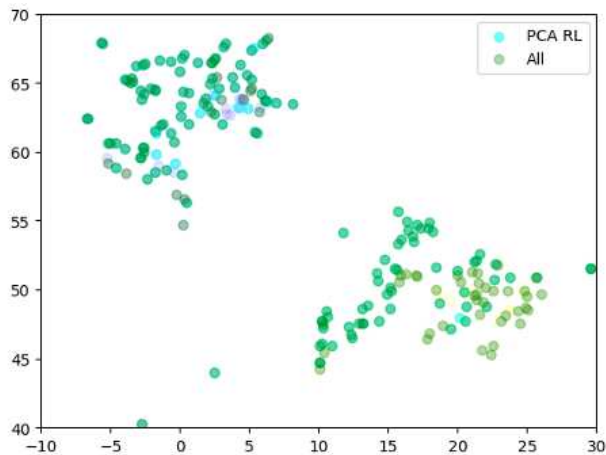


Figure 10. Zoomed-in view of TSNE 2D representation of distribution of dataset points upon the PCA manifold $M = 84$ showing those detected by PCA RE and those by all the on-manifold models combined. The points in cyan are anomalies that are only detected by the off-manifold method.

Fig. 7 and gives the distribution of points representing 1s (in red), 7s (blue) and 8s (yellow).

In Fig 8 we plot the points we have detected as anomalies using the reconstruction error method. We can see that the reconstruction error approach performs reasonably well at identifying the “islands” of both 7s and 8s.

As discussed previously, we used various unsupervised AD methods – LOF, EllipticEnvelope, One-Class SVM, and Isolation Forest – on the PCA generated manifold to find outlying points; and then combined them with IF and PCA Reconstruction to test AD recall, and these results are shown in Table 3.

We also combined PCA $M = 84$ reconstruction error with a combination of IF and LOF and this achieved a recall of 85% (cf. 78.8% for IF-LOF) and precision 44.9% (cf. 44.7% for IF-LOF), showing again the value of combining on and off-manifold techniques.

Even when *all* the on-manifold methods were combined for the PCA $M = 84$ manifold, there were still some anomalies which are detected by the off-manifold method which the combination of on-manifold methods do not detect (the points shown in cyan in Fig. 10).

Distribution of the anomalies detected on the t-SNE representation are shown in Fig 13.

G.3.2. AE MANIFOLDS

This work was then repeated using AEs. AE manifolds were built using Keras (Tensorflow) (Chollet et al., 2015) with one hidden layer in each of the encoder and decoder. The dimensionalities of the AE manifolds were $M=245$ ($M \lesssim D$, c.f. $D=784$) and $M=30$. The latter was following Geron (2023) enabling us to use only 30 dimensions for the latent space and still satisfy the manifold hypothesis.

Using reconstruction error to identify anomalies, the distribution of MSE for the dataset is shown in Fig. 14.

The distribution of the 1s, 7s and 8s on a t-SNE view of the $M = 30$ AE manifold is shown in Fig. 12. Note how the 2D representation of the manifold is not identical to that of the PCA manifold shown in Fig. 7, demonstrating how the manifold construction is model dependent.

We then employed the same methods that were used with PCA to perform AD on the AE manifolds. We computed recall and precision for these techniques standalone and in conjunction with AE reconstruction error based approach, as previously discussed and as shown in Table 4.

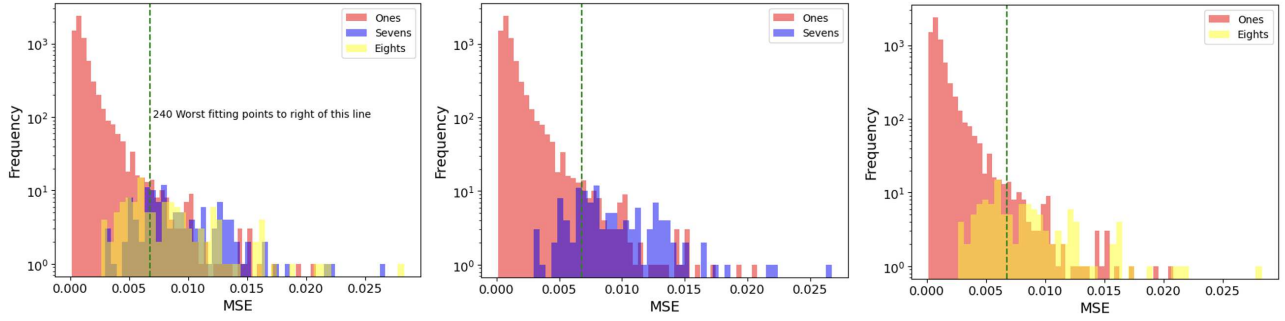


Figure 11. MSE of reconstruction error between PCA manifold and original data representations. Anomalies are defined as the most outlying 240 points

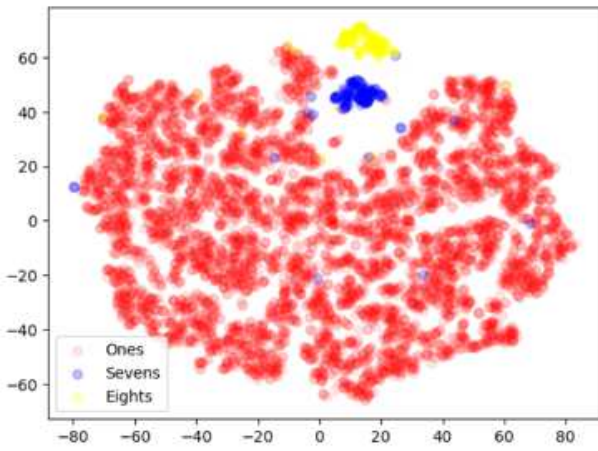


Figure 12. Chart showing distribution of different underlying data classes on t-SNE 2D representation of the AE $M = 30$ manifold

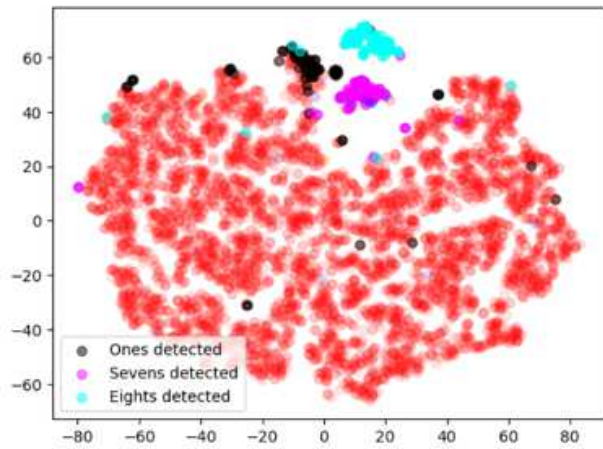


Figure 13. Chart showing distribution of anomalies detected through AE reconstruction error from the AE $M = 30$ manifold

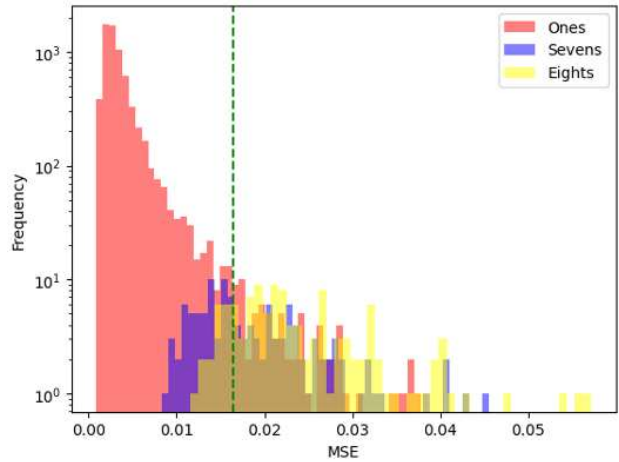


Figure 14. Chart showing MSE between reconstruction and original data from AE generated manifold